inorganics

MDPI

Article

[2 × 2] Molecular Grids of Ni(II) and Zn(II) with Redox-Active 1,4-Pyrazine-Bis(thiosemicarbazone) Ligands

Natalia Arefyeva [1], Aaron Sandleben [1], Alexander Krest [1], Ulrich Baumann [2], Mathias Schäfer [3], Maxim Kempf [4] and Axel Klein [1,*]

1 Department für Chemie, Institut für Anorganische Chemie, Universität zu Köln, Greinstraße 6, D-50939 Köln, Germany; narefyev@uni-koeln.de (N.A.); a.sandleben@uni-koeln.de (A.S.); alexander@krest.de (A.Kr.)
2 Department für Chemie, Institut für Biochemie, Universität zu Köln, Otto-Fischer-Str. 12-14, D-50674 Köln, Germany; ubaumann@uni-koeln.de
3 Department für Chemie, Zentrum für Massenspektrometrie, Institut für Organische Chemie, Universität zu Köln Greinstraße 4, D-50939 Köln, Germany; aco78@uni-koeln.de
4 Department für Chemie, Institut für Physikalische Chemie, Universität zu Köln, Luxemburger Str. 116, 50939 Köln, Germany; maxim.kempf@uni-koeln.de
* Correspondence: axel.klein@uni-koeln.de; Tel.: +49-221-470-4006

Received: 19 April 2018; Accepted: 17 May 2018; Published: 21 May 2018

Abstract: Tetranuclear complexes $[M_4(L^R)_4]$ with M = Ni(II) or Zn(II), with a [2 × 2] grid-type structure, were assembled in good yields and purity from the easily accessible but unprecedented pyrazine-bridged bis(thiosemicarbazone) protoligands (ligand precursors) H_2L^R (1,4-pyrazine-2,5-bis(R-carbaldehyde-thiosemicarbazone); R = Me, Et, ^{i}Pr, or Ph). The complexes were characterised in solution by NMR, MS, IR, and UV-Vis absorption spectroscopy and (spectro)electrochemical methods. HR-MS spectra unequivocally reveal that the tetranuclear species are very stable in solution and any measurements represent these species. Only at higher temperatures (fragmentation in solution: MS and in the solid: TG-DTA) or upon the addition of protons (acidic UV-Vis titrations) can the tetrameric entities be decomposed. Single crystal XRD measurement remained preliminary. Rapid loss of co-crystallised solvent molecules within the [2 × 2] grid-type structures resulted in crystals of very poor quality, but the results were qualitatively in line with spectroscopy, electrochemistry, and quantum chemical (DFT) calculations. IR and NMR spectroscopy point clearly to a thiolate coordination of dianionic (deprotonated) ligands. The electrochemistry reveals four electronically coupled and reversible one-electron reductions centred largely at the pyrazine bridges. EPR and UV-Vis spectroelectrochemical measurements in combination with DFT calculation support the assignment.

Keywords: bis(thiosemicarbazone); 1,4-pyrazine; supramolecular chemistry; mass spectrometry; electrochemistry

1. Introduction

Thiosemicarbazons and their metal complexes are studied intensely since the 1950s, mainly for their interesting biological properties. Antitumor, antibacterial, antiviral, and antifungal effects have been reported [1–11]. A general formula for a thiosemicarbazone (Scheme 1A) reveals a chelate NˆS binding pocket for the coordination to metals. However, many of the so far reported thiosemicarbazones carry a heteroaryl substituent R. The frequently used 2-pyridyl group thus

opens the possibility of a tridentate N_{Py}–N–S coordination with two five-ring chelates on the metal (Scheme 1B) [7–10].

Bi- or oligonuclear transition metal complexes of thiosemicarbazone ligands have been obtained frequently through S-bridging of the thiosemicarbazone ligands [3,4,8,12–20]. Systematic formation of bi- or oligonuclear complexes through ligand design has successfully used functionalised mono-thiosemicarbazone ligands, such as the 2-(di(pyridyl-2-yl)thiosemicarbazone [13,21] or bis(thiosemicarbazone) ligands [4,5,9,20–27]. For example, pyridine-2,6-bis(thiosemicarbazones) (Scheme 1C) have been synthesised to provide a potential SˆNˆNˆNˆS coordination for the metal [4,10,22,28,29] and were found to form binuclear complexes through S-bridging [22,29], but they largely fail to bridge two metal centres due to their preference for multi-dentate binding [4,10,22,28].

Remarkably, among the arene bis(thiosemicarbazones) ligands, there are only a few in which bifunctional heterocyclic arene units directly connect two (M-arene-M) or more metals. The only examples are some 1,2,4-triazole-bridged cyclometalated Pd or Pt complexes [25–27] and three binuclear pyrazole-bridged Co(II), Ni(II), and Zn(II) complexes, which have not been structurally characterised (XRD) [30]. Interestingly, the above-mentioned 1,2,4-triazole-brigded bis(thiosemicarbazone) ligands frequently tend to form binuclear Pt(II) or Pd(II) complexes showing the S-bridging mode [31] rather than an M-N1(triazole)N2-M or M-N1(triazole)N4-M bridge [26,31].

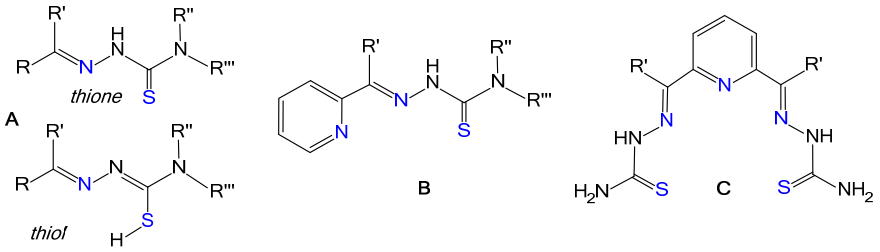

Scheme 1. Schematic representation of thiosemicarbazones (**A**), 2-acetylpyridine-thiosemicarbazones (**B**), and 2,6-diacetylpyridine-bis(thiosemicarbazone) (**C**) with various substituents.

This brought us to the idea to synthesise the potentially bridging 1,4-pyrazine-bis(thiosemicarbazone) ligands shown in Scheme 2 and we were amazed that this ligand motive has not been reported before. In contrast to this, 1,4-pyrazine-*mono*-thiosemicarbazone ligands and complexes have been frequently reported [32–38] including the application as topoisomerase IIa inhibitor [36].

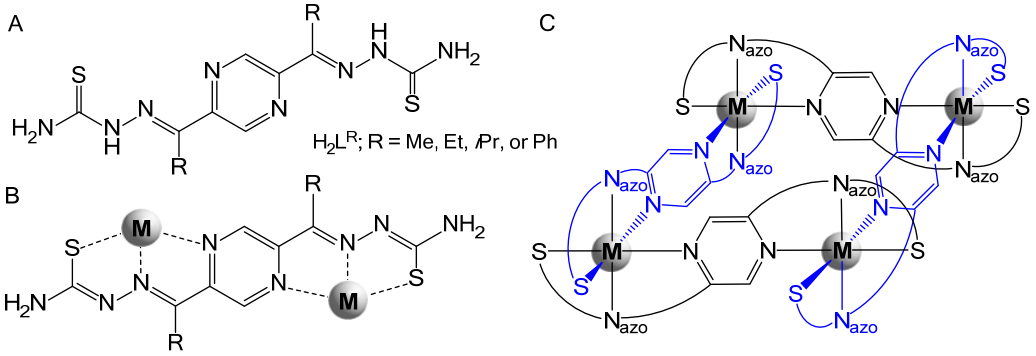

Scheme 2. The 1,4-pyrazine-bridged bis(thiosemicarbazone) protoligands (ligand precursor) H_2L^R with R = Me (L^{Me}), Et (L^{Et}), ^{i}Pr (L^{iPr}), or Ph (L^{Ph}) used in this study (**A**); the dianionic ligands $(L^R)^{2-}$ bridging two metals (**B**); the assumed tetrameric products obtained in this study (**C**).

1,4-Pyrazine has previously shown to be a very suitable ligand to bridge two metal centres and provide effective electronic coupling between the two atoms [39–42]. The Creutz-Taube ion

$[(NH_3)_5Ru(\mu\text{-}1,4\text{-pyrazine})Ru(NH_3)_5]^{5+}$ is probably the most prominent example for this [40,42]. Our idea was to combine the interesting electronic properties of 1,4-pyrazine with the stable binding of the tridentate arene-thiosemicarbazone framework (Scheme 2).

Having thus synthesised four new 1,4-pyrazine-bridged bis(thiosemicarbazones) H_2L^R (R = Me, Et, ^{i}Pr, Ph) (Scheme 2), we reacted them with Ni(II) or Zn(II) salts to explore their coordination chemistry. We obtained tetranuclear complexes $[M_4(L^R)_4]$ (M = Ni or Zn) with a [2 × 2] grid-type structure in high yields (Scheme 2). Similarly, so-called [2 × 2] metallogrid like complexes have been synthesised using suitable multitopic ligands [43,44]. Many of them contain the heteroaromatic central metal–metal bridging units pyrimidine [43–48], or pyrazolate [43,44,49–52]. The use of *s*-triazine [43] and pyridazine [43,44] as a central moiety has been frequently reported, while examples with imidazole [52–54], tetrazine [55,56], and 1,4-pyrazine [45,46,57–60] are scarce. These tetranuclear complexes have found interest from their magnetic and redox properties [41,43,44,51,59,60].

In this contribution, we report the synthesis of four new 1,4-pyrazine-bridged bis(thiosemicarbazones) H_2L^R and their tetranuclear complexes $[M_4(L^R)_4]$ (M = Ni or Zn). Detailed spectroscopic and electrochemical characterisation reveals that a number of specific topics render these new metallosquares remarkable.

2. Results and Discussion

2.1. Synthesis and Characterisation

Synthesis of the protoligands (protonated ligand precursors) H_2L^R. For the synthesis of the pyrazine-2,5-carbaldehydes (R = Me, Et, ^{i}Pr, or Ph), we modified a literature procedure [61] converting aldehydes to the corresponding radicals by a Fenton type reaction (Scheme 3 left), and 1,4-pyrazine was then added (details in the Supplementary Materials). After formation the pyrazine-2,5-carbaldehydes precipitate from the reaction, yields were only moderate (~35%). The yellow pyrazine-2,5-carbaldehydes were reacted with thiosemicarbazide (Scheme 3, right) to produce the bis(thiosemicarbazone) protoligands H_2L^R in good yield (63–90%).

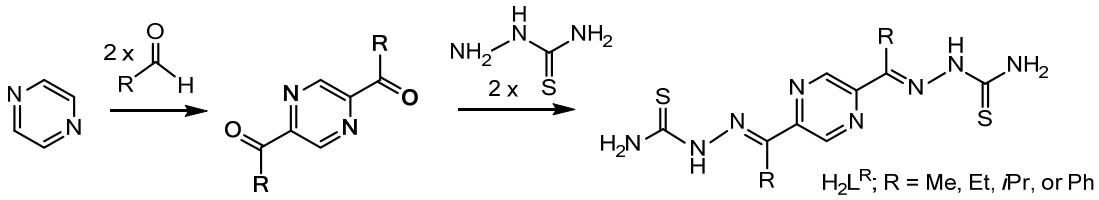

Scheme 3. Synthesis of the 1,4-pyrazine-bridged bis(thiosemicarbazone) protoligands (ligand precursor) H_2L^R with R = Me (L^{Me}), Et (L^{Et}), ^{i}Pr (L^{iPr}), or Ph (L^{Ph}).

Synthesis and analysis of the complexes. The protoligands H_2L^R were dissolved in DMA (*N*,*N*-dimethylacetamide) and KOH dissolved in EtOH was added. This mixture was layered carefully using a 0.01 M solution of $[Zn(acac)_2]$ ($acac^-$ = acetylacetonate) dissolved in MeCN. From many solvents, we tried DMA was best to prevent any precipitation during this procedure. Careful crystallisation over one or two weeks yielded red microcrystalline materials (details in the experimental section). Corresponding reactions using $Ni(BF_4)_2$ yielded dark blue materials. Yields for the eight new compounds were good (45–75%), and the solubility of the products in organic solvents was generally low; they were air- and moisture-stable. Elemental analysis gave M:L ratios of 1:1 in the products, and the anionic thiolate form of the ligand was confirmed by IR spectroscopy. For example, the azoN–H function disappeared, and strong vibrations in the range 1200 to 1400 cm^{-1} represent the increasing double bond character in the –N=C(S)(NH_2) unit of the deprotonated ligand [9]. Consequently, the C=S stretching mode shifts from about 840 cm^{-1} to values ranging from 730 to 780 cm^{-1}, indicative of the coordinated thiolate form in the complexes. NMR spectroscopy was

carried out on the protoligands H_2L^R but failed on most of the Zn(II) complexes due to low solubility. For the Ni(II) derivatives, the paramagnetic behaviour precluded meaningful NMR experiments (figures in the Supplementary Materials).

Mass spectrometry unequivocally revealed the presence of tetranuclear complexes in solutions of $[M_4(L^R)_4]$ (Figures 1 and 2). Positive ionisation mass spectra ESI(+)-MS of all samples in acetone show peaks corresponding to $[[M_4(L^R)_4]+H]^+$, $[[M_3(L^R)_3]+H]^+$, $[[M_2(L^R)_2]+H]^+$, and in some spectra even dicationic tetranuclear species $[[M_4(L^R)_4]+2H]^{2+}$ (Figure 2). Similar observations have been reported from related Ni_4 [55,56,62–66] or Zn_4 [58,59,66] [2 × 2] grids showing surprisingly high stability.

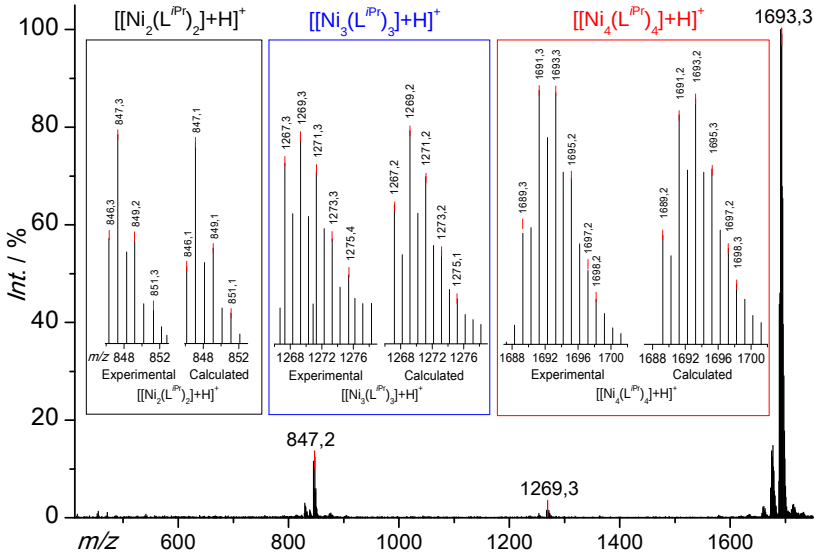

Figure 1. ESI-MS (pos.) of $[Ni_4(L^{iPr})_4]$ obtained from an acetone solution. The inserts show the fragments corresponding to the binuclear, trinuclear, and tetranuclear species (from left to right) with simulations.

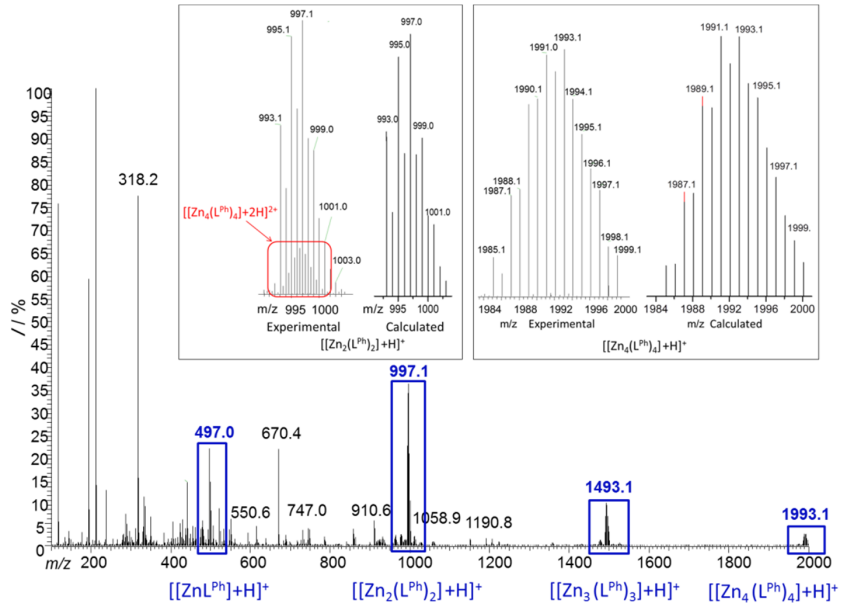

Figure 2. ESI-MS (pos.) of $[Zn_4(L^{Ph})_4]$ obtained from an acetone solution. The inserts show the fragments corresponding to the dimer (left), and tetramer (right) with simulations. Marked in red (top left) is the isotopic pattern of the dicationic tetrameric fragment $[Zn_4(L^{Ph})_4]+2H]^{2+}$.

2.2. Properties of the Solids

TG-DTA measurements on the bulk solid materials are in line with the tetrameric character and reveal up to two molecules DMA and in all cases four molecules H_2O adherent to the tetrameric units from recrystallisation (figures in the Supplementary Materials) in line with the elemental analyses (see Experimental Section). Up to about 250 °C, the volatile H_2O and DMA molecules evaporate, followed by an exothermic decomposition cleaving the $NH_2C(S)N$ fragments, which can be concluded from a mass-loss of about 30–35%. Crystal and molecular structures could not be obtained yet. From the complexes, $[M_4(L^R)_4]$ single crystals were obtained and submitted to X-ray diffraction experiments. Unfortunately, most of the structure solutions were of low quality. High R_{int} values point to low crystal quality, which is probably due to solvent molecules in the lattice. The best obtained structure solution could be carried out for $[Ni_4(L^{iPr})_4]$, details on the structure solution can be found in the Supplementary Materials.

The tetrameric molecular structure revealed by Figure 3 is fully in line with HR-MS, further spectroscopies, electrochemistry, and quantum chemical calculations (see later), which makes us confident that, although the structure solution is very poor, the structure is essentially correct.

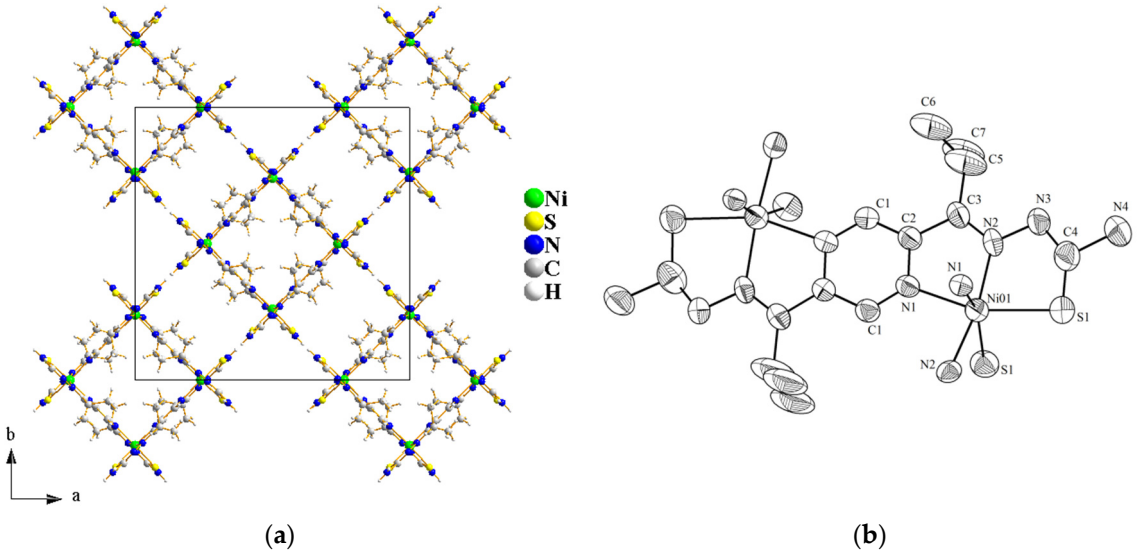

(**a**) (**b**)

Figure 3. Crystal structure of $[Ni_4(L^{iPr})_4]$ at 293(2) K, solved in the tetragonal space group *I*422 (R_{int} = 0.0937, R_1 solved (all data) = 0.1087 (0.1611); wR_2 = 0.3048 (0.3617) viewed along the crystallographic *c* axis (**a**) and an ORTEP plot of the binuclear coordination unit (**b**) shown at 50% probability level; protons were omitted for clarity.

2.3. UV-Vis Absorption Spectroscopy

The coordination of the protoligands H_2L^R to Ni(II) and Zn(II) under deprotonation can be also traced in the UV-Vis absorption spectra. While the protoligands H_2L^R having a –C(R)=N–NH–C(=S)NH_2 configuration exhibit intense long-wavelength absorption maxima up to about 400 nm (Table S4 in the ESI), the Zn(II) complexes show markedly red-shifted intra-ligand absorptions up to 550 nm (Figure 4) in line with a $(L^R)^{2-}$ –C(R)=N–N=C(–S)NH_2 motive (compare Scheme 2).

These quite intense long-wavelength bands (ε > 20,000 $M^{-1}\cdot cm^{-1}$) are also in line with the red colour of the Zn(II) containing materials. The maxima of the even more intense (ε > 40,000 $M^{-1}\cdot cm^{-1}$) long-wavelength bands of the Ni(II) complexes exceed 600 nm (Figure 4) in line with the blue colour of the materials. Due to their similar appearance, the long-wavelength bands in both Zn(II) and Ni(II) complexes were assigned to intra-ligand absorptions. For the Ni(II) complexes additional absorptions can be observed as very long-wavelength shoulders around 700 nm, they might be assigned to nickel(d) to pyrazine(π^*) metal-to-ligand charge transfer (MLCT) transitions.

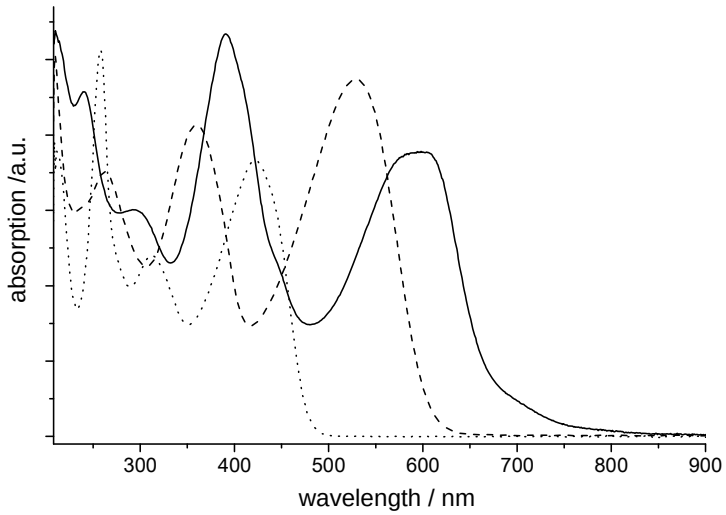

Figure 4. UV-Vis absorption spectra of H_2L^{iPr} (dotted line), $[Zn_4(L^{iPr})_4]$ (dashed line), and $[Ni_4(L^{iPr})_4]$ (solid line) in THF.

To probe the stability of the compounds against acids UV-Vis titrations were carried out for $[Zn_4(L^{iPr})_4]$ and $[Ni_4(L^{iPr})_4]$. To THF solutions of the complexes (4×10^{-5} mol in 2 mL: 22 mmol/L) aliquots of conc. acetic acid (HOAc) were added and spectral changes were recorded. Upon the addition of up to 12 aliquots (210 mmol), the long-wavelength bands at >500 nm largely bleach, while the intense bands at around 380 nm reveal a slight blue-shift and a slight gain in intensity (Figure S32 in the Supplementary Materials). Importantly, there are clearly isosbestic points and the spectra changes are completely reversed upon the addition of small amounts of solid KOH. Upon the addition of further amounts of HOAc both absorption bands vanish and the underlying transformation cannot be completely reversed. We assume that the stability of the tetranuclear species in solution decreases within the series $[M_4(L^R)_3(HL^R)]^+ >> [M_4(L^R)_2(HL^R)_2]^{2+} > [M_4(L^R)(HL^R)_3]^{3+} > [M_4(HL^R)_4]^{4+}$, but still the $[M_4(L^R)_4]$ complex can be reconstituted. The larger extent of protonation, e.g., to yield $[M_4(HL^R)_3(H_2L^R)]^{5+}$ probably leads to an irreversible disintegration. Unfortunately, the same tests in water, allowing for a quantitative description using the pK_A value of HOAc and measuring the basicity of $[M_4(L^R)_4]$, were prevented by the poor solubility of the compounds in water.

2.4. Electrochemistry

The electrochemical behaviour of the protoligands and the complexes was studied by cyclic voltammetry (CV) and square-wave voltammetry (SQW). Figure 5 shows examples, Table 1 summarises the redox potentials. The tetranuclear complexes exhibit four consecutive one-electron reduction steps in the range of -1.4 to -2 V, which are completely reversible on the timescale of the experiment. In the same range, the protoligands H_2L^R show one reversible reduction. Thus, the pyrazine moiety seems largely to be the target for these reduction processes [33,39,40,42], although some variation of the potentials stems from the R substituents. In the tetranuclear complexes, we thus assign the first four waves to successive one-electron reduction of the four pyrazine moieties. We assume that the second reduction occurs to the pyrazine moiety opposite to the firstly reduced pyrazine group, similar to what has been described for the four Fe(II)/Fe(III) oxidation processes in the [2 × 2] grid $[Fe_4(L)_4]$ (HL = 4-methyl-3,5-bis{6-(2,2′-bipyridyl)} pyrazole [51]. The differences between first and second reduction potentials (ΔE) as well as between the third and fourth reduction potentials are around 110 mV, while the second and third reduction potentials differ about 300 mV. Remarkably, this is regardless of the incorporated metal. Unfortunately, the irreversibility of the second reductions for the protoligands H_2L^R precludes the exact calculation of the differences ΔE, but the values surely exceed 200 mV (Table 1).

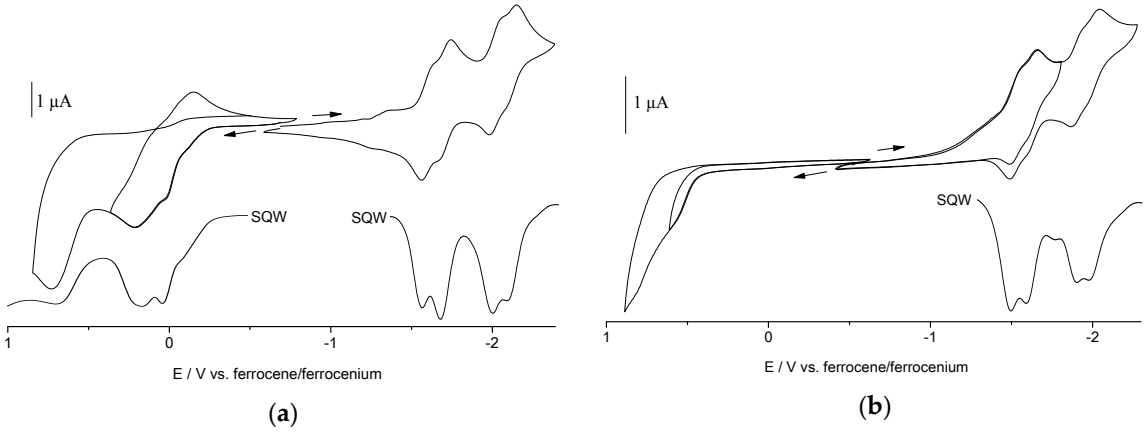

Figure 5. Cyclic voltammograms and square-wave voltammograms (SQWs) of the complexes $[Ni_4(L^{iPr})_4]$ (**a**) and $[Zn_4(L^{iPr})_4]$ (**b**) in $^{n}Bu_4NPF_6$/THF solution at 298 K and 20 mV/s scan rate; potentials/V vs. ferrocene/ferrocenium.

Table 1. Selected electrochemical data for H_2L^R and tetrameric complexes $[M_4(L^R)_4]$ [1].

			E_{pa} ox1	$E_{1/2}$ red1	E_{pc} red2	E_{pc} red3	E_{pc} red4
H_2L^{Me}	-	-	-	−1.69	−2.05	−2.62	−2.81
H_2L^{Et}	-	-	0.62	−1.67	−2.13	−2.75	−3.25
H_2L^{iPr}	-	-	0.60	−1.63	−2.11	−2.51	−2.66
H_2L^{Ph}	-	-	0.50	−1.48	−1.70	−1.97	−2.45
	E_{pa} ox3	E_{pa} ox2	E_{pa} ox1	$E_{1/2}$ red1	$E_{1/2}$ red2	$E_{1/2}$ red3	$E_{1/2}$ red4
$[Zn_4(L^{iPr})_4]$	-	0.80	0.55	−1.54	−1.65	−1.93	−2.03
$[Zn_4(L^{Ph})_4]$	-	0.79	0.53	−1.41	−1.52	−1.86	−1.91
$[Ni_4(L^{Et})_4]$	-	0.21	0.04	−1.47	−1.56	−1.82	−1.95
$[Ni_4(L^{iPr})_4]$	0.72	0.21	0.02	−1.59	−1.71	−2.02	−2.13
$[Ni_4(L^{Ph})_4]$	0.80	0.32	0.29	−1.43	−1.54	−1.82	−1.94

[1] From cyclic voltammetry in 0.1 M $^{n}Bu_4NPF_6$/THF solutions at 100 mV/s or 20 mV/s scan rate. Potentials in V vs. ferrocene/ferrocenium. Half-wave potentials $E_{1/2}$ for reversible or partially reversible processes; anodic (E_{pa}) or cathodic (E_{pc}) peak potentials for irreversible processes.

We can conclude that, in the [2 × 2] grid arrangement of the tetranuclear complexes $[M_4(L^R)_4]$, the four pyrazine moieties are electronically connected, allowing one to determine four separate waves and thus the observation of three mixed-valent states. The stability constants $K_C = 10^{(\Delta E/59mV)}$ [40,42] are about 10^2 for the first product of reduction $[M_4(L^R)_3(L^{R\bullet})]^{\bullet-}$ and about 10^5 for $[M_4(L^R)_2(L^{R\bullet})_2]^{2-}$. A metal-mediated electronic coupling through empty d orbitals can be ruled out since the values for Ni(II) having an empty dx^2-y^2 orbital and for Zn(II) having no empty d orbital are much the same. Instead, the four crystallographically and spectroscopically identical pyrazine moieties are electronically connected through spacial proximity, as has been reported for a number of rectangular $[\{Re(CO)_3\}_4(\mu\text{-}X)_2(\mu\text{-}L)_2]$ (X = thiolate, alkoxide [67]; X/2 = 2,2′-bisbenzimidazolate [68] or octahydro-2,2′-bipyrimidine) [69] complexes with heteroaromatic bridging ligands such as 1,4-pyrazine or 4,4′-bipyridine. Depending on the plane-to-plane distance, the potential splitting ΔE for the pyrazine systems lie between 200 (larger than 5.5 Å) [68,69] and 450 mV (around 4 Å) [67]. Interestingly, even for the weakly coupled system (X/2 = 2,2′-bisbenzimidazolate) [68] with a 250 mV separation a weak intervalence charge transfer (IVCT) absorption was observed at 5350 cm^{-1} (1870 nm; ε = 150 $M^{-1}\cdot cm^{-1}$) for the first reduced mixed-valent state, for stronger coupled systems having shorter ligand-to-ligand distances, these bands can be quite pronounced [67,68,70].

In the mononuclear Ga(III) complexes $[Ga(L)_2]^+$ containing two neighbouring pyrazine thiosemicarbazonate ligands, two ligand-centred one-electron reductions were observed at about

−1.3 V and −1.5 V, respectively, with separations ΔE ~270 mV [33]. For the Fe(III) derivatives $[Fe(L)_2]^+$, the reductions lie at around −1.9 V and −2.3 V, respectively, revealing larger separation ΔE ~420 mV. Importantly, a first reduction of the $[Fe(L)_2]^+$ complexes can be assigned to a Fe(II)/Fe(III) couple, thus these ligand-centred reductions occur to neutral Fe(II) complexes $[Fe(L)_2]$ [33]. For these Ga and Fe complexes, third reduction waves have been observed at potentials of about −2.2 V (Ga) and −2.8 V (Fe), respectively, and a fourth reduction has been observed at around −2.5 V for the Ga derivatives. The third waves lie over 600 mV lower than the second, indicative of the second reduction of a pyrazine moiety [39,40]. For these complexes, the first two reductions occur thus successively to the two metal-connected pyrazine-thiosemicarbazone ligands, the third and fourth reduction waves represent the second reduction of these units [33]. The larger ΔE observed for the Fe(II) d^6 low spin systems [33] points to an efficient electronic coupling of the two pyrazine moieties through empty metal d orbitals. However, for Ga(III) d^{10}, such a mechanism can be ruled out. ΔE is smaller but still appreciable. Thus, also here, in line with our findings, a through-space electronic interaction can be postulated for the two pyrazine units.

The second reduction of the four pyrazine moieties in our complexes $[M_4(L^R)_4]^{4-} \rightarrow [M_4(L^R)_4]^{5-/6-/7-/8-}$ are expected to occur at potentials approximately 600–700 mV lower (more negative) and were not detected unequivocally in our experiments due to the overlap with solvent and water (co-crystallised) discharge waves.

There are a number of irreversible oxidation waves at around +0.5 V both in the protoligands H_2L^R and the Zn complexes, which were assigned to oxidations at the thiol(ate) group of the thiosemicarbazone moiety. For the Ni(II) complexes, additional Ni(II)/Ni(III) couples were observed at even lower potentials. Due to the irreversible nature of all of these processes, the assignment remains preliminary.

2.5. Spectroelectrochemical UV-Vis Absorption and EPR Spectroscopy

UV-Vis absorption spectra were recorded during cathodic electrolysis of the two complexes $[M_4(L^{iPr})_4]$ (M = Ni or Zn). For M = Ni, Figure 6 shows a continuous change of the spectra during the first two reduction steps (left part) with no evidence for a defined mixed-valent species $[Ni_4(L^{iPr})_4]^{\bullet-}$, especially no intervalence charge transfer (IVCT) band [39,40,42,67,68,70], in line with the far higher stability constant K_C of 10^5 for $[M_4(L^{iPr})_2(L^{iPr\bullet})_2]^{2-}$ compared with 10^2 for $[M_4(L^{iPr})_3(L^{iPr\bullet})]^{\bullet-}$. At −1.9 V, the observed process (first and second reduction), which goes along with a blue-shift of the two dominating bands at 605 (to 565 nm) and 392 (to 371 nm) and the appearance of a weaker double maximum at 694 and 635 nm is completed (Figure 6a).

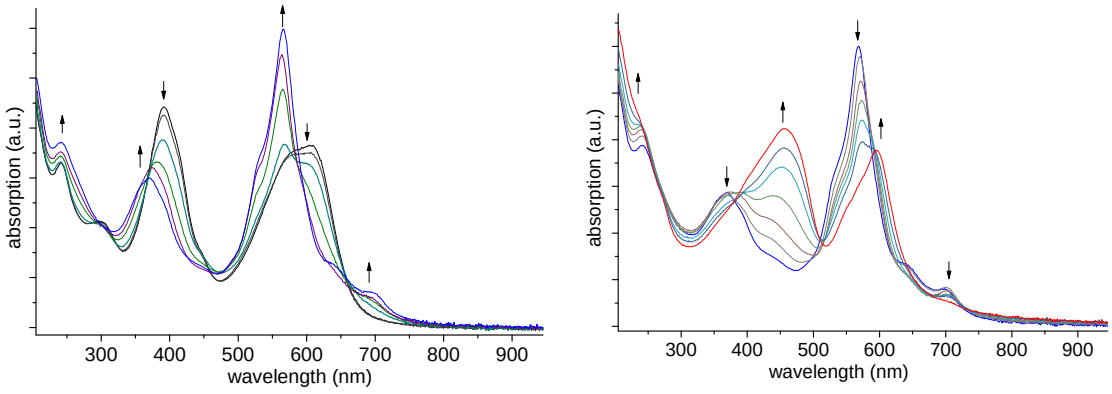

(**a**) (**b**)

Figure 6. UV-Vis absorption spectra recorded during cathodic reduction of $[Ni_4(L^{iPr})_4]$ in THF/^{n}Bu$_4$NPF$_6$ solutions. (**a**) Spectra recorded at E = 0 and from −1.5 to −1.9 V; (**b**) spectra recorded from E = −2.0 to −2.6 V.

Further reduction (third and fourth reduction) also results in continuous changes, such as the disappearance of the two long-wavelength weak absorptions and the red-shift of the two intense bands in the visible range (Figure 6b). Again, we found no evidence for a mixed-valent species $[Ni_4(L^{iPr})_4]^{\bullet 3-}$, probably again due to the far higher stability of the $[Ni_4(L^{iPr})_4]^{4-}$ state. For the Zn derivative, the behaviour is very similar (spectra in the Supplementary Materials).

For the weakly coupled rectangular $[\{Re(CO)_3\}_4(\mu\text{-}X)_2(\mu\text{-}L)_2]]$ (X/2 = 2,2′-bis-benzimidazolate [68] system with a 250 mV separation ΔE, a weak intervalence absorption band was observed at 5350 cm^{-1} (1870 nm; ε = 150 $M^{-1}\cdot cm^{-1}$) for the first reduced mixed-valent state. At the same time, there are ligand mixed-valent systems containing similar ligand face-to-face moieties and pronounced separations ΔE, where no intervalence bands were detected [71,72].

A detailed look on our spectra reveals that isosbestic points are far from being perfect. This might be due to the fact that more than two species were observed, thus a weak hint for the mixed-valent species. At the same time, the spectra of the highly reduced species show some long-wavelength tailing, indicative of a precipitation of these highly charged complexes. In line with this, the full reversibility of the first four reduction processes through re-oxidation is only obtained upon long standing at 0 V.

X-band EPR spectra recorded during cathodic electrolysis of $[Ni_4(L^{iPr})_4]$ at potentials between −1.5 and −1.9 V (first and second reduction) gave an isotropic signal at g = 2.016 with only 45 G total spectral width (Figure S40). This is in line with a pyrazine-centred radical complex, and no indication for a second reduced species was found.

2.6. Quantumchemical Calculations

DFT calculations were initiated to obtain insight on the energy and location of the highest occupied molecular orbital (HOMO) and the lowest unoccupied molecular orbital (LUMO) of the complexes. First, we calculated the molecular structures of the complexes in the gas phase on (RI-)BP86/def-SV(P) level and refined some of the resulting structures on (RI-)BP86/def2-TZVP level. Frequency calculations were carried out in order to check for the absence of imaginary frequencies, which confirms an energetic minimum for the geometry. The calculated minimum geometries agree quite well with the experimental structures from HR-MS in solution and with the preliminary single crystal XRD results (Tables S5 and S6).

The calculated LUMOs (Figures 7a and 8a) are largely centred on the pyrazine units in line with the EPR results but also the CNNCN chain of the thiosemicarbazonate contributes markedly, in line with the dependency of the reduction potentials on the R substituents. Importantly, there was no indication of an electronic coupling of the four pyrazine units, in line with the assumed electrostatic nature of the observed splitting of the four reduction waves.

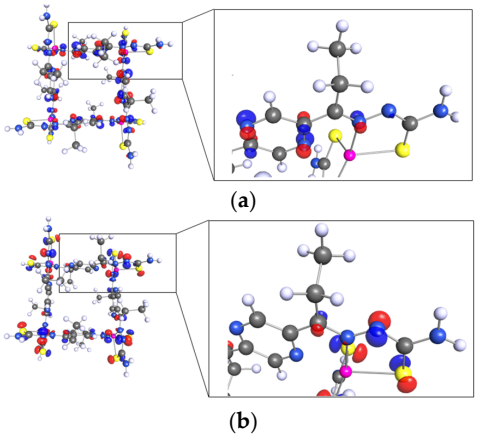

Figure 7. DFT (RI-)BP86/def2-TZVP calculated LUMO (**a**) and HOMO (**b**) of $[Zn_4(L^{Et})_4]$.

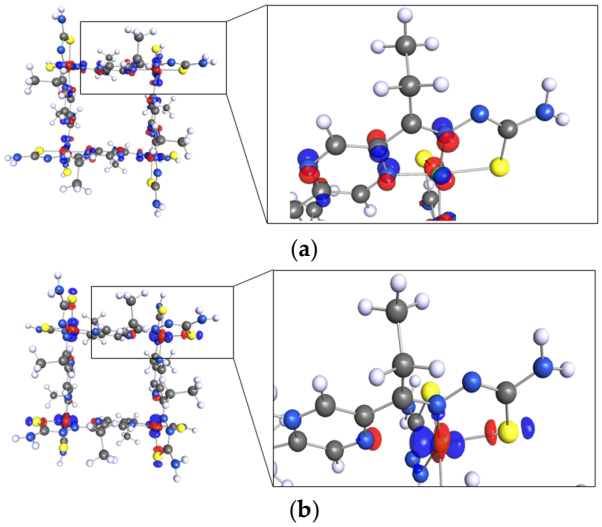

Figure 8. DFT (RI-)BP86/def2-TZVP calculated LUMO (**a**) and HOMO (**b**) of $[Ni_4(L^{Et})_4]$.

The largest contributions to the calculated HOMOs come from the thiolate S atoms. However, while both S atoms contribute in the same way for the Zn(II) complex (Figure 7b), for the Ni(II) system d orbital contributions were visible in the electron density plots (Figure 8b) seemingly replacing one of the S atom contributions. This is in line with a d orbital control of the coordination in the case of d^8 Ni(II) in contrast to the rather spherical coordination of d^{10} Zn(II) [73]. The nature of the calculated HOMOs is also in agreement with the assignment of the observed oxidation waves.

3. Experimental Section

3.1. Methods and Instrumentation

Elemental analysis was obtained using a HEKAtech CHNS EuroEA 3000 Analyzer (HEKAtech GmbH, Wegberg, Germany). The NMR spectra were recorded on a Bruker Avance II 300 MHz (Bruker, Rheinfelden, Germany) (^{1}H: 300.13 MHz, ^{13}C: 75.47 MHz)—double resonance (BBFO) 5 mm observe probehead with a z-gradient coil or on a Bruker Avance II 600 MHz spectrometer (Bruker, Rheinfelden, Germany) (^{1}H: 600.13 MHz, ^{13}C: 150.93 MHz, ^{15}N: 60.83 MHz)—triple resonance (TBI) 5 mm inverse probehead with a z-gradient coil. The unambiguous assignment of the ^{1}H, ^{13}C, and ^{15}N resonances was obtained from ^{1}H COSY, ^{1}H NOESY, gradient selected ^{1}H, ^{13}C HSQC, and HMBC, and gradient selected ^{1}H and ^{15}N HMBC experiments. All 2D NMR experiments were performed using standard pulse sequences from the Bruker pulse program library. Chemical shifts were relative to TMS for ^{1}H and ^{13}C and to CH_3NO_2 for ^{15}N. The spectra analyses were performed by the *Bruker TopSpin 3.2* software. UV-Vis absorption spectra were measured on Varian Cary50 Scan or Shimadzu UV-3600 photo spectrometers (Shimadzu Deutschland, Duisburg, Germany). Electrochemical experiments were carried out in 0.1 M THF solutions using a three-electrode configuration (glassy carbon working electrode, Pt counter electrode, and Ag/AgCl pseudo reference) and an Autolab PGSTAT30 potentiostat (Metrohm, Filderstadt, Germany) and function generator. The ferrocene/ferrocenium couple ($FeCp_2/FeCp_2^+$) served as an internal reference. UV-Vis spectroelectrochemical measurements were performed with an optically transparent thin-layer electrochemical (OTTLE) cell [42]. EI-MS spectra were measured with a Finnigan MAT 900 S (MasCom, Bremen, Germany). ESI-MS spectra were recorded on a Bruker Daltonics Esquire 3000 plus (Bruker, Rheinfelden, Germany) and HRMS-ESI spectra were obtained on a Thermo Scientific LTQ Orbitrap XL and LTQ Orbitrap hybrid instrument (Thermo Fisher Scientific Waltham, MA, USA). Simulations were performed using *ISOPRO* 3.0 programme (M. Senko, download from https//sites.google.com). FT-IR (Fourier transform infrared) analyses have been carried out using a Perkin Elmer-Spectrum 400 (PerkinElmer, Waltham, MA,

USA) coupled with a Universal ATR Sampling Accessory in the 400–4000 cm^{-1} range. TG-DTA measurements were carried out using a TGA/DSC 1 STAR system by Mettler Toledo (Greifensee, Zürich, Schweiz). Single crystal structure XRD measurements were performed at 293(2) or 170(2) K using graphite-monochromatised Mo-Kα radiation (λ = 0.71073 Å) on IPDS II (STOE and Cie). The structures were solved by direct methods using SIR 2011 [74] or SIR 92 [75], and refinement was carried out with SHELXL 2013 [76] or SHELXL 97 [77] employing full-matrix least-squares methods on F^2 with ${F_0}^2 \geq 2\sigma({F_0}^2)$. The numerical absorption corrections using *X-RED* V1.22 (Stoe & Cie, 2001) [78,79] were performed after optimising the crystal shapes using *X-SHAPE* V1.06 (Stoe & Cie, 1999) [78,79]. Non-hydrogen atoms were refined with anisotropic displacement parameters. H atoms were included using appropriate riding models. The refined tetranuclear structures contained additional disordered solvate molecules. Because no reasonable split model was found, the data were corrected for disordered solvent using the SQUEEZE option in *PLATON* [80,81]. The R_{int} and the refined R_1 and wR_2 values were generally poor and A level alerts were found in Platon checkcif. Since this includes even data obtained at 170(2) K, we can ascribe this to the generally very low quality of the crystals. We assume that they rapidly decompose upon evaporation of the solvent molecules in the voids (see elemental analyses and thermogravimetric analyses). CCDC 1484512 ($[Ni_4(L^{Me})_4]\cdot H_2O$) 1484515 ($[Ni_4(L^{Me})_4]$), 1484516 ($[Ni_4(L^{Et})_4]\cdot H_2O$), 1484517 ($[Ni_4(L^{iPr})_4]$), 1435303 ($[Zn_4(L^{iPr})_4]$), and 1435304 ($[Zn_4(L^{Ph})_4]$) contain the full crystallographic data for this paper. These data can be obtained free of charge from The Cambridge Crystallographic Data Centre via www.ccdc.cam.ac.uk/data_request/cif. Selected single crystal structure determinations were carried out at the Swiss Light Source (SLS), Paul Scherrer Institute (PSI), Villigen, Switzerland, on beamline X06DA (PXIII, MAR225 CCD). Crystals were mounted in nylon loops and flash-cooled in liquid nitrogen. Data were collected at 100 K. The wavelength was tuned to 0.7205 Å and a Pilatus 2M detector was employed. Data were collected in two wedges of 120 degrees each with Chi angles on the PRIGo goniostat (PSI) [82] set to 0 and 30 degrees, respectively. Data were processed with *XDS* and *XSCALE* [83]. Computational details: Ground state electronic structure calculations on complexes were performed on the basis of density-functional theory (DFT) methods with resolution of identity coulomb approximation [84] using the *TURBOMOLE* 6.6 and 7.0 [85] program packages and the *TMoleX* 4.1 [86] user interface. For all atoms, the double-ξ-valence def-SVP [87] and the triple-ξ-valence def2-TZVP [88] basis sets were used with *Becke's* gradient-corrected exchange-energy functional BP86 [89].

3.2. Syntheses

3.2.1. General

General information on materials and details on the synthesis of the pyrazine-2,5-carbaldehydes and the bis(thiosemicarbazones) H_2L^R (R = Me, Et, ^{i}Pr, Ph) are provided in the Supplementary Materials.

3.2.2. Synthesis of the tetranuclear complexes $[M_4(L^R)_4]$

General description: To the protoligands H_2L^R dissolved in DMA 0.01 M (1 equiv), we added a 0.044 M solution of KOH (0.2 equiv) in EtOH. This solution was layered carefully using 1 equiv of a 0.01 M solution of the corresponding metal salt ($Ni(BF_4)_2$ or $[Zn(acac)_2]$ in MeCN. The reaction mixtures were left to crystallise taking one to two weeks. The materials were filtered off and washed with water and dried at 70 °C or under vacuum. Despite this drying procedure, we found varying amounts of DMA and/or water in the elemental analyses, thermogravimetric analyses, and NMR spectra.

$[Ni_4(L^{Me})_4]$: Dark blue crystals. Yield: 82.6 mg (0.06 mmol, 45%). Anal. Calc. for $[Ni_4(L^{Me})_4]\cdot 4DMA$ $C_{56}H_{84}N_{36}Ni_4O_4S_8$: C, 37.02; H, 4.66; N, 27.75; S, 14.12; Found: C, 37.25; H, 4.53; N, 27.71; S, 13.82%. MS (ESI, *m*/*z*): 1469 $[M + H]^+$, FT-IR: 3435 w(br), 3279 m(br), 3107 m(br), 2923 w, 2869 w, 1595 s, 1541 s, 1493 m, 1385 s, 1352 s, 1288 s, 1223 m, 1196 w, 1150 s, 1126 s(br), 1029 w(br), 898 w(br), 786 m, 700 w, 592 w cm^{-1}. UV-Vis (THF, λ_{max}): 578, 385, 295 nm.

$[Ni_4(L^{Et})_4]$: Dark blue crystals. Yield: 148.2 mg (0.09 mmol, 75%). Anal. Calc. for $[Ni_4(L^{Et})_4]\cdot 4DMA\cdot 4H_2O$ $C_{64}H_{108}N_{36}Ni_4O_8S_8$: C, 38.41; H, 5.44; N, 25.20; S, 12.82; Found: C, 38.27; H, 5.44; N, 25.14; S, 12.57%. MS (ESI, *m*/*z*): 1581 $[M + H]^+$, FT-IR: 3435 w(br), 3279 m(br), 3155 m(br), 2971 w, 2934 w, 2874 w, 1595 s, 1536 m, 1504 w, 1369 s, 1310 m, 1288 s, 1228 m, 1207 w, 1153 m, 1110 s(br), 1064 w, 1036 w, 1013 w, 942 m, 829 m, 754 w, 705 m, 592 m cm^{-1}. UV-Vis (THF, λ_{max}): 605, 444sh, 391, 294sh nm.

$[Ni_4(L^{iPr})_4]$: Dark blue crystals. Yield: 152.4 mg (0.09 mmol, 75%). Anal. Calc. for $C_{56}H_{80}N_{32}S_8Ni_4$: C, 39.74; H, 4.76; N, 26.48; S, 15.15; Found: C, 39.68; H, 4.74; N, 26.24; S, 15.33%. MS (ESI, *m*/*z*): 1693 $[M + H]^+$, FT-IR: 3462 w(br), 3274 m(br), 3149 m(br), 2966 w, 2928 w, 2874 w, 1585 s, 1520 w, 1498 w, 1461 w, 1358 s, 1272 s, 1223 m, 1171 w, 1110 s(br), 1035 w, 980 m, 759 m, 700 m, 587 w cm^{-1}. UV-Vis (THF, λ_{max}): 604, 575sh, 444sh, 413sh, 391, 240, 214 nm.

$[Ni_4(L^{Ph})_4]$: Dark blue crystals. Yield: 122.8 mg (0.06 mmol, 50%). Anal. Calc. for $C_{80}H_{64}N_{32}Ni_4S_8$: C, 48.90; H, 3.28; N, 22.81; S, 13.06; Found: C, 48.53; H, 3.48; N, 22.72; S, 12.79%. MS (ESI, *m*/*z*): 1965 $[M + H]^+$, FT-IR: 3446 w(br), 3274 m(br), 3155 m(br), 1585 s, 1528 w, 1488 m, 1443 w, 1347 s(br), 1282 s, 1239 s, 1185 m, 1115 s(br), 958 m, 905 w, 845 w, 797 m, 737 m, 694 s, 645 w, 581 w, 548 w cm^{-1}. UV-Vis (THF, λ_{max}): 623, 585sh, 450sh, 421sh, 395, 277 nm.

$[Zn_4(L^{Et})_4]$: Dark red crystals. Yield: 112.5 mg (0.07 mmol, 56%). Anal. Calc. for $[Zn_4(L^{Et})_4]\cdot 4DMA\cdot 4H_2O$ $C_{64}H_{108}N_{36}O_8S_8Zn_4$: C, 37.91; H, 5.37; N, 24.87; S, 12.65; Found: C, 37.86; H, 5.35; N, 24.67; S, 12.37%. MS (ESI, *m*/*z*): 1607 $[M + H]^+$, FT-IR: 3427 w(br), 3270 m(br), 3153 m(br), 2980 w, 2933 w, 2874 w, 1626 m, 1597 s, 1537 w, 1504 w, 1445 w, 1361 s, 1285 s, 1226 m, 1201 w, 1154 m, 1124 s(br), 1036 w, 935 m, 821 m, 741 s, 694 s, 589 m, 471 w cm^{-1}. UV-Vis (THF, λ_{max}): 551, 368, 277 nm.

$[Zn_4(L^{iPr})_4]$: Dark red crystals. Yield: 113.9 mg (0.07 mmol, 53%). Anal. Calc. for $[Zn_4(L^{iPr})_4]\cdot 4DMA\cdot 4H_2O$ $C_{72}H_{124}N_{36}O_8S_8Zn_4$: C, 40.41; H, 5.84; N, 23.56; S, 11.99; Found: C, 40.40; H, 5.75; N, 23.42; S, 11.59%. MS (ESI, *m*/*z*): 1719, 1721 $[M + H]^+$, FT-IR: 3414 w, 3283 m(br), 3153 m(br), 2962 w, 2933 w, 2857 w, 1589 m, 1525 w, 1491 w, 1457 w, 1361 s, 1272 s, 1221 m, 1116 s(br), 1032 w, 973 w, 875 w, 838 w, 753 m, 694 m, 593 w, 517 w cm^{-1}. UV-Vis (THF, λ_{max}): 528, 360, 262 nm.

$[Zn_4(L^{Ph})_4]$: Dark red crystals. Yield: 112.0 mg (0.06 mmol, 45%). Anal. Calc. for $C_{80}H_{64}N_{32}S_8Zn_4$: C, 48.25; H, 3.24; N, 22.50; S, 12.88; Found: C, 48.27; H, 3.66; N, 22.48; S 12.65%. ^{1}H-NMR (600 MHz, DMSO-d_6) δ [ppm]: 7.74 (s, 8H, H_{pyz}), 7.64–7.55 (m, 40H, H_{ph}), 6.78 (s, 16H, H_{NH2}); MS (ESI, *m*/*z*): 1991, 1993 $[M + H]^+$, FT-IR: 3443 w(br), 3275 w(br), 3148 w(br), 1592 m, 1496 w, 1373 s, 1293 s, 1234 s, 1183 w, 1112 s(br), 1028 w, 956 m, 846 w, 783 w, 736 w, 690 m, 610 w, 539 w cm^{-1}. UV-Vis (THF, λ_{max}): 532, 392, 253 nm.

4. Conclusions

Tetranuclear complexes $[M_4(L^R)_4]$ with M = Ni(II) or Zn(II), with a so-called [2 × 2] grid-type structure were assembled from the new and versatile pyrazine-bridged bis(thiosemicarbazone) protoligands H_2L^R (1,4-pyrazine-2,5-bis(R-carbaldehyde-thiosemicarbazone; R = Me, Et, ^{i}Pr, or Ph) in good yields and purity.

HR-MS spectra unequivocally reveal that the tetranuclear species are very stable and any measurements in solution represent these species. Only at higher temperatures (fragmentation in MS) or upon addition of protons (acidic UV-Vis titrations), the tetrameric entities are decomposed. In the solid, they are stable up to 250 °C as revealed by TG-DTA measurements. TG-DTA also revealed rapid loss of co-crystallised solvent molecules within the [2 × 2] grid-type structures, which also resulted in a single crystal of very poor quality. Thus, single crystal XRD measurement remained preliminary. However, the results were qualitatively in line with spectroscopy, electrochemistry, and quantum chemical (DFT) calculations. IR spectroscopy points clearly to a thiolate coordination of dianionic (deprotonated) ligands. The electrochemistry reveals four electronically coupled and reversible one-electron reductions centred at the four pyrazine moieties. The data give no indication for a metal-mediated electronic coupling, thus ligand–ligand interaction through space (= supramolecular)

was concluded for the pronounced splitting of the reduction waves (up to 300 mV). EPR and UV-Vis spectroelectrochemical measurements fail to detect specific spectra of the mixed-valent species $[M_4(L^R)_4]^{\bullet -}$ and $[M_4(L^R)_4]^{\bullet 3-}$ indicative of relatively weak (largely electrostatic) coupling. DFT calculations support these assignments.

In future work, we will study the properties of these new materials in more detail. Especially, we will try to obtain better crystal and molecular structures from single-crystal XRD and explore potential applications, e.g., in multi-electron catalysis. Furthermore, we will expand the coordination chemistry of these new and easy-to-make 1,4-pyrazine-2,5-bis(thiosemicarbazone) ligands. Especially, the electronic connection of various low-valent metals through the 1,4-pyrazine unit might yield materials with interesting optoelectronic properties such as intense absorptions in the visible and NIR for light harvesting. Additionally, the cooperative effects of two connected metals in catalytic applications will be studied.

Supplementary Materials: The following are available online at http://www.mdpi.com/2304-6740/6/2/51/s1. (A) Experimental section details, (B) Figures S1–S40: NMR, MS, IR spectra, crystal and molecular structures, UV-Vis absorption spectra and voltammograms of complexes, Table S1: Selected crystallographic and structure refinement data for $[M_4(L^R)_4]$ (M = Ni or Zn) Tables S2 and S3: Selected bond lengths /Å and bond angles /° of Ni and Zn complexes, Table S4: Absorption maxima of the H_2L^R protoligands and the Zn and Ni complexes, Tables S5 and S6: Selected DFT-calculated and experimental bond lengths /Å and bond angles /° of Zn and Ni complexes. Tables S7–S13: Atom coordinates of calculated molecule structures of complexes $[M_4(L^R)_4]$ (M = Ni or Zn). (C) Cif and Checkcif file of the complexes.

Author Contributions: N.A. carried out synthesis and analysis of the compound. N.A., A.Kr., and U.B. collected data and solved and refined XRD datasets. A.S. performed the quantum chemical calculations. M.S. and M.K. carried out HR-MS spectroscopy. A.Kl. designed the project and wrote the manuscript. All authors have given approval to the final version of the manuscript.

Acknowledgments: We thank Ingo Pantenburg (University of Cologne) for crystal data collection and Daniela Naumann for her support with NMR measurement. Rainer Winter, University of Konstanz, is acknowledged for fruitful discussions. U.B. thanks the European Community's Seventh Framework Programme (FP7/2007-2013) under BioStruct-X (grant agreement N°283570). The staff of the beamline X06SA at the Paul Scherrer Institute, SLS, Villigen, Switzerland is acknowledged for assistance during data collection. APC was sponsored by MDPI.

Conflicts of Interest: The authors declare no conflict of interest.

References

1. Jansson, P.J.; Kalinowski, D.S.; Lane, D.J.R.; Kovacevic, Z.; Seebacher, N.A.; Fouani, L.; Sahne, S.; Merlot, A.M.; Richardson, D.R. The renaissance of polypharmacology in the development of anti-cancer therapeutics: Inhibition of the "Triad of Death" in cancer by Di-2-pyridylketone thiosemicarbazones. *Pharmacol. Res.* **2015**, *100*, 255–260. [CrossRef] [PubMed]
2. Lane, D.J.R.; Mills, T.M.; Shafie, N.H.; Merlot, A.M.; Moussa, R.S.; Kalinowski, D.S.; Kovacevic, Z.; Richardson, D.R. Expanding horizons in iron chelation and the treatment of cancer: Role of iron in the regulation of ER stress and the epithelial–mesenchymal transition. *Biochim. Biophys. Acta* **2014**, *1845*, 166–181. [CrossRef] [PubMed]
3. Dilworth, J.R.; Hueting, R. Metal complexes of thiosemicarbazones for imaging and therapy. *Inorg. Chim. Acta* **2012**, *389*, 3–15. [CrossRef]
4. Paterson, B.M.; Donnelly, P.S. Copper complexes of bis(thiosemicarbazones): From chemotherapeutics to diagnostic and therapeutic radiopharmaceuticals. *Chem. Soc. Rev.* **2011**, *40*, 3005–3018. [CrossRef] [PubMed]
5. Ettari, R.; Bova, F.; Zappala, M.; Grasso, S.; Micale, N. Falcipain-2 Inhibitors. *Med. Res. Rev.* **2010**, *30*, 136–167. [CrossRef] [PubMed]
6. Pelosi, G.; Bisceglie, F.; Bignami, F.; Ronzi, P.; Schiavone, P.; Re, M.C.; Casoli, C.; Pilotti, E. Antiretroviral Activity of Thiosemicarbazone Metal Complexes. *J. Med. Chem.* **2010**, *53*, 8765–8769. [CrossRef] [PubMed]
7. Pelosi, G. Thiosemicarbazone Metal Complexes: From Structure to Activity. *Open Cryst. J.* **2010**, *3*, 16–28. [CrossRef]
8. Lobana, T.S.; Sharma, R.; Bawa, G.; Khanna, S. Bonding and structure trends of thiosemicarbazone derivatives of metals-An overview. *Coord. Chem. Rev.* **2009**, *253*, 977–1055. [CrossRef]

9. Christlieb, M.; Dilworth, J.R. Ligands for Molecular Imaging: The Synthesis of Bis(thiosemicarbazone) Ligands. *Chem.-Eur. J.* **2006**, *12*, 6194–6206. [CrossRef] [PubMed]
10. Quiroga, A.G.; Ranninger, C.N. Contribution to the SAR field of metallated and coordination complexes. Studies of the palladium and platinum derivatives with selected thiosemicarbazones as antitumoral drugs. *Coord. Chem. Rev.* **2004**, *248*, 118–133. [CrossRef]
11. Baartzes, N.; Stringer, T.; Okombo, J.; Seldon, R.; Warner, D.F.; de Kock, C.; Smith, P.J.; Smith, G.S. Mono- and polynuclear ferrocenylthiosemicarbazones: Synthesis, characterisation and antimicrobial evaluation. *J. Organomet. Chem.* **2016**, *819*, 166–172. [CrossRef]
12. Indoria, S.; Lobana, T.S.; Singh, D.; Kumari, S.; Kumari, P.; Bala, T.; Kamal, A.; Jassal, A.K.; García Santos, I.; Castineiras, A.; et al. Stabilization of Cu^{II}–I Bonds Using 2-Benzoylpyridine Thiosemicarbazones—Synthesis, Structure, Spectroscopy, Fluorescence, and Cyclic Voltammetry. *Eur. J. Inorg. Chem.* **2015**, *2015*, 5106–5117. [CrossRef]
13. Qi, J.; Liang, S.; Gou, Y.; Zhang, Z.; Zhou, Z.; Yang, F.; Liang, H. Synthesis of four binuclear copper(II) complexes: Structure, anticancer properties and anticancer mechanism. *Eur. J. Med. Chem.* **2015**, *96*, 360–368. [CrossRef] [PubMed]
14. Shao, J.; Bao, W.-G.; Tian, H.; Li, B.; Zhao, X.-F.; Qiao, X.; Xu, J.-Y. Nuclease activity and protein-binding properties of a novel tetranuclear thiosemicarbazide Pt(II) complex. *Dalton Trans.* **2014**, *43*, 1663–1671. [CrossRef] [PubMed]
15. Pereira, M.T.; Antelo, J.M.; Adrio, L.A.; Martinez, J.; Ortigueira, J.M.; Lopez-Torres, M.; Vila, J.M. Novel Bidentate [*N*,*S*] Palladacycle Metalloligands. $^{1}H-^{15}N$ HMBC as a Decisive NMR Technique for the Structural Characterization of Palladium−Rhodium and Palladium−Palladium Bimetallic Complexes. *Organometallics* **2014**, *33*, 3265–3274. [CrossRef]
16. Adams, M.; de Kock, C.; Smith, P.J.; Chibale, K.; Smith, G.S. Synthesis, characterization and antiplasmodial evaluation of cyclopalladated thiosemicarbazone complexes. *J. Organomet. Chem.* **2013**, *736*, 19–26. [CrossRef]
17. Demoro, B.; de Almeida, R.F.M.; Marques, F.; Matos, C.P.; Otero, L.; Pessoa, J.C.; Santos, I.; Rodríguez, A.; Moreno, V.; Lorenzo, J.; et al. Screening organometallic binuclear thiosemicarbazone ruthenium complexes as potential anti-tumour agents: Cytotoxic activity and human serum albumin binding mechanism. *Dalton Trans.* **2013**, *42*, 7131–7146. [CrossRef] [PubMed]
18. Ali, A.A.; Nimir, H.; Aktas, C.; Huch, V.; Rauch, U.; Schäfer, K.-H.; Veith, M. Organoplatinum(II) Complexes with 2-Acetylthiophene Thiosemicarbazone: Synthesis, Characterization, Crystal Structures, and in Vitro Antitumor Activity. *Organometallics* **2012**, *31*, 2256–2262. [CrossRef]
19. Chellan, P.; Land, K.M.; Shokar, A.; Au, A.; An, S.H.; Clavel, C.M.; Dyson, P.J.; de Kock, C.; Smith, P.J.; Chibale, K.; et al. Exploring the Versatility of Cycloplatinated Thiosemicarbazones as Antitumor and Antiparasitic Agents. *Organometallics* **2012**, *31*, 5791–5799. [CrossRef]
20. Latheef, L.; Seena, E.B.; Kurup, M.R.P. Synthesis, spectral and structural studies of novel binuclear Ni(II) complex of salicylaldehyde 3-azacyclothiosemicarbazone. *Inorg. Chim. Acta* **2009**, *362*, 2515–2518. [CrossRef]
21. Philip, V.; Suni, V.; Kurup, M.R.P.; Nethaji, M. Copper(II) complexes derived from di-2-pyridyl ketone *N*(4),*N*(4)-(butane-1,4-diyl)thiosemicarbazone: Crystal structure and spectral studies. *Polyhedron* **2006**, *25*, 1931–1938. [CrossRef]
22. Panja, A.; Campana, C.; Leavitt, C.; Van Stipdonk, M.J.; Eichhorn, D.M. Iron and cobalt complexes of 2,6-diacetylpyridine-bis(R-thiosemicarbazone) (R = H, phenyl) showing unprecedented ligand deviation from planarity. *Inorg. Chim. Acta* **2009**, *362*, 1348–1354. [CrossRef] [PubMed]
23. Pedrido, R.; Gonzalez-Noya, A.M.; Romero, M.J.; Martinez-Calvo, M.; Vazquez Lopez, M.; Gomez-Forneas, E.; Zaragoza, G.; Bermejo, M.R. Pentadentate thiosemicarbazones as versatile chelating systems. A comparative structural study of their metallic complexes. *Dalton Trans.* **2008**, *47*, 6776–6787. [CrossRef] [PubMed]
24. Matsinha, L.C.; Mao, J.; Mapolie, S.F.; Smith, G.S. Water-Soluble Palladium(II) Sulfonated Thiosemicarbazone Complexes: Facile Synthesis and Preliminary Catalytic Studies in the Suzuki–Miyaura Cross-Coupling Reaction in Water. *Eur. J. Inorg. Chem.* **2015**, *2015*, 4088–4094. [CrossRef]
25. Matesanz, A.I.; Tapia, S.; Souza, P. First 3,5-diacetyl-1,2,4-triazol derived mono(thiosemicarbazone) and its palladium and platinum complexes: Synthesis, structure and biological properties. *Inorg. Chim. Acta* **2016**, *445*, 62–69. [CrossRef]

26. Matesanz, A.I.; Perles, J.; Souza, P. New palladium and platinum complexes with bioactive 3,5-diacetyl-1,2,4-triazol bis(4-cyclohexyl thiosemicarbazone) ligand: Chemistry, antiproliferative activity and preliminary toxicity studies. *Dalton Trans.* **2012**, *41*, 12538–12547. [CrossRef] [PubMed]
27. Matesanz, A.I.; Pastor, C.; Souza, P. Synthesis and structural characterization of a disulphide-bridged tetranuclear palladium(II) complex derived from 3,5-diacetyl 1,2,4-triazole bis(4-ethylthiosemicarbazone). *Inorg. Chem. Commun.* **2007**, *10*, 97–100. [CrossRef]
28. Kasuga, N.C.; Sekino, K.; Koumo, C.; Shimada, N.; Ishikawa, M.; Nomiya, K. Synthesis, structural characterization and antimicrobial activities of 4- and 6-coordinate nickel(II) complexes with three thiosemicarbazones and semicarbazone ligands. *J. Inorg. Biochem.* **2001**, *84*, 55–65. [CrossRef]
29. De Sousa, G.F.; West, D.X.; Brown, C.A.; Swearingen, J.K.; Valdes-Martinez, J.; Toscano, R.A.; Hernandez-Ortega, S.; Hörner, M.; Bortoluzzi, A.J. Structural and spectral studies of a heterocyclic *N*(4)-substituted bis(thiosemicarbazone), $H_2$2,6Achexim·H_2O, its heptacoordinated tin(IV) complex [Bu_2Sn(2,6Achexim)], and its binuclear zinc(II) complex [Zn(2,6Achexim)]$_2$. *Polyhedron* **2000**, *19*, 841–847. [CrossRef]
30. Kulkarni, N.V.; Revankar, V.K. Synthesis, antimicrobial screening, and DNA-binding/cleavage of new pyrazole-based binuclear Co^{II}, Ni^{II}, Cu^{II}, and Zn^{II} complexes. *J. Coord. Chem.* **2011**, *64*, 725–741. [CrossRef]
31. Matesanz, A.I.; Hernandez, C.; Rodriguez, A.; Souza, P. Novel bis(thiosemicarbazones) of the 3,5-diacetyl-1,2,4-triazol series and their platinum(II) complexes: Chemistry, antiproliferative activity and preliminary nephrotoxicity studies. *Dalton Trans.* **2011**, *40*, 5738–5745. [CrossRef] [PubMed]
32. Drover, M.W.; Tandon, S.S.; Anwar, M.U.; Shuvaev, K.V.; Dawe, L.N.; Collins, J.L.; Thompson, L.K. Polynuclear complexes of a series of hydrazone and hydrazone–oxime ligands—M_2 (Fe), M_4 (Mn, Ni, Cu), and Mn (Cu) examples. *Polyhedron* **2014**, *68*, 94–102. [CrossRef]
33. Kowol, C.R.; Reisner, E.; Chiorescu, I.; Arion, V.B.; Galanski, M.; Deubel, D.V.; Keppler, B.K. An Electrochemical Study of Antineoplastic Gallium, Iron and Ruthenium Complexes with Redox Noninnocent α-N-Heterocyclic Chalcogensemicarbazones. *Inorg. Chem.* **2008**, *47*, 11032–11047. [CrossRef] [PubMed]
34. Kowol, C.R.; Berger, R.; Eichinger, R.; Roller, A.; Jakupec, M.A.; Schmidt, P.P.; Arion, V.B.; Keppler, B.K. Gallium(III) and Iron(III) Complexes of α-*N*-Heterocyclic Thiosemicarbazones: Synthesis, Characterization, Cytotoxicity, and Interaction with Ribonucleotide Reductase. *J. Med. Chem.* **2007**, *50*, 1254–1265. [CrossRef] [PubMed]
35. Li, M.-X.; Zhang, L.-Z.; Yang, M.; Niu, J.-Y.; Zhou, J. Synthesis, crystal structures, in vitro biological evaluation of zinc(II) and bismuth(III) complexes of 2-acetylpyrazine *N*(4)-phenylthiosemicarbazone. *Bioorg. Med. Chem. Lett.* **2012**, *22*, 2418–2423. [CrossRef] [PubMed]
36. Zeglis, B.M.; Divilov, V.; Lewis, J.S. Role of Metalation in the Topoisomerase IIα Inhibition and Antiproliferation Activity of a Series of α-Heterocyclic-*N*4-Substituted Thiosemicarbazones and Their Cu(II) Complexes. *J. Med. Chem.* **2011**, *54*, 2391–2398. [CrossRef] [PubMed]
37. Li, M.; Sun, Q.; Bai, Y.; Duan, C.; Zhang, B.; Meng, Q. Chiral aggregation and spontaneous resolution of thiosemicarbazone metal complexes. *Dalton Trans.* **2006**, 2572–2578. [CrossRef] [PubMed]
38. West, D.X.; Bain, G.A.; Butcher, R.J.; Jasinski, J.P.; Pozdniakiv, R.Y.; Valdes-Martinez, J.; Toscano, R.A.; Hernandez-Ortega, S. Structural Studies of three Isomeric Forms of Heterocyclic *N*(4)-Substituted Thiosemicarbazones and two Nickel(II) Complexes. *Polyhedron* **1996**, *15*, 665–674. [CrossRef]
39. Kaim, W.; Sarkar, B.; Lahiri, G.K. *Mixed Valence Intermediates as Ideal Targets für Spectroelectrochemistry in Spectroelectrochemistry*; Kaim, W., Klein, A., Eds.; RSC Publishing: Cambridge, UK, 2008; Chapter 3; pp. 68–90. ISBN 978-0-85404-550-1. [CrossRef]
40. Kaim, W.; Klein, A.; Glöckle, M. Exploration of Mixed-Valence Chemistry: Inventing New Analogues of the Creutz-Taube Ion. *Acc. Chem. Res.* **2000**, *33*, 755–763. [CrossRef] [PubMed]
41. Ferrando-Soria, J.; Vallejo, J.; Castellano, M.; Martínez-Lillo, J.; Pardo, E.; Cano, J.; Castro, I.; Lloret, F.; Ruiz-García, R.; Julve, M. Molecular magnetism, quo vadis? A historical perspective from a coordination chemist viewpoint. *Coord. Chem. Rev.* **2017**, *339*, 17–103. [CrossRef]
42. Kaim, W.; Fiedler, J. Spectroelectrochemistry: The best of two worlds. *Chem. Soc. Rev.* **2009**, *38*, 3373–3382. [CrossRef] [PubMed]
43. Hardy, J.G. Metallosupramolecular grid complexes: Towards nanostructured materials with high-tech applications. *Chem. Soc. Rev.* **2013**, *42*, 7881–7899. [CrossRef] [PubMed]

44. Dawe, L.N.; Shuvaev, K.V.; Thompson, L.K. Polytopic ligand directed self-assembly—Polymetallic [$n \times n$] grids *versus* non-grid oligomers. *Chem. Soc. Rev.* **2009**, *38*, 2334–2359. [CrossRef] [PubMed]
45. Stefankiewicz, A.R.; Lehn, J.-M. Highly Sensitive Magnetic Effects Induced by Hydrogen-Bonding Interactions in a High-Spin Metallosupramolecular Fe_4^{II} [2 × 2] Grid-Type Complex. *Chem. Eur. J.* **2009**, *15*, 2500–2503. [CrossRef] [PubMed]
46. Shen, F.; Huang, W.; Wu, D.; Zheng, Z.; Huang, X.-C.; Sato, O. Redox Modulation of Spin Crossover within a Cobalt Metallogrid. *Inorg. Chem.* **2016**, *55*, 902–908. [CrossRef] [PubMed]
47. Wu, S.-Q.; Wang, Y.-T.; Cui, A.-I.; Kou, H.-Z. Toward Higher Nuclearity: Tetranuclear Cobalt(II) Metallogrid Exhibiting Spin Crossover. *Inorg. Chem.* **2014**, *53*, 2613–2618. [CrossRef] [PubMed]
48. Wang, Y.-T.; Li, S.-T.; Wu, S.-Q.; Cui, A.-L.; Shen, D.-Z.; Kou, H.-Z. Spin Transitions in Fe(II) Metallogrids Modulated by Substituents, Counteranions, and Solvents. *J. Am. Chem. Soc.* **2013**, *135*, 5942–5945. [CrossRef] [PubMed]
49. Steinert, M.; Schneider, B.; Dechert, S.; Demeshko, S.; Meyer, F. Spin-State Versatility in a Series of Fe_4 [2 × 2] Grid Complexes: Effects of Counteranions, Lattice Solvent, and Intramolecular Cooperativity. *Inorg. Chem.* **2016**, *55*, 2363–2373. [CrossRef] [PubMed]
50. Tong, J.; Demeshko, S.; John, M.; Dechert, S.; Meyer, F. Redox-Induced Single-Molecule Magnetism in Mixed-Valent [2 × 2] Co_4 Grid Complexes. *Inorg. Chem.* **2016**, *55*, 4362–4372. [CrossRef] [PubMed]
51. Schneider, B.; Demeshko, S.; Neudeck, S.; Dechert, S.; Meyer, F. Mixed-Spin [2 × 2] Fe_4 Grid Complex Optimized for Quantum Cellular Automata. *Inorg. Chem.* **2013**, *52*, 13230–13237. [CrossRef] [PubMed]
52. Yang, H.; Cao, F.; Li, D.; Zeng, S.; Song, Y.; Dou, J. Solvent dependent reactivities of di-, tetra- and hexanuclear manganese complexes: Syntheses, structures and magnetic properties. *Dalton Trans.* **2015**, *44*, 6620–6629. [CrossRef] [PubMed]
53. Matsumoto, T.; Newton, G.N.; Shiga, T.; Hayami, S.; Matsui, Y.; Okamoto, H.; Kumai, R.; Murakami, Y.; Oshio, H. Programmable spin-state switching in a mixed-valence spin-crossover iron grid. *Nat. Commun.* **2014**, *5*, 3865. [CrossRef] [PubMed]
54. Li, X.; Wu, B.; Wang, R.; Zhang, H.; Niu, C.; Niu, Y.; Hou, H. Hierarchical Assembly of Extended Coordination Networks Constructed by Novel Metallacalix[4]arenes Building Blocks. *Inorg. Chem.* **2010**, *49*, 2600–2613. [CrossRef] [PubMed]
55. Campos-Fernandez, C.S.; Schottel, B.L.; Chifotides, H.T.; Bera, J.K.; Bacsa, J.; Koomen, J.M.; Russell, D.H.; Dunbar, K.R. Anion Template Effect on the Self-Assembly and Interconversion of Metallacyclophanes. *J. Am. Chem. Soc.* **2005**, *127*, 12909–12923. [CrossRef] [PubMed]
56. Campos-Fernandez, C.S.; Clerac, R.; Dunbar, K.R. A One-Pot, High-Yield Synthesis of a Paramagnetic Nickel Square from Divergent Precursors by Anion Template Assembly. *Angew. Chem. Int. Ed.* **1999**, *38*, 3477–3479. [CrossRef]
57. Li, X.-L.; Kang, J.-L.; Zhang, X.-L.; Xiao, H.-P.; Wang, A.-L.; Zhou, L.; Fang, S.-M.; Liu, C.-M. Anion-controlled self-assembly of two NLO-active dinuclear and molecular square Cu(II) enantiomeric pairs: From antiferromagnetic to ferromagnetic coupling. *Dalton Trans.* **2014**, *43*, 17226–17229. [CrossRef] [PubMed]
58. Bark, T.; Düggeli, M.; Stoeckli-Evans, H.; von Zelewsky, A. Designed Molecules for Self-Assembly: The Controlled Formation of Two Chiral Self-Assembled Polynuclear Species with Predetermined Configuration. *Angew. Chem. Int. Ed.* **2001**, *40*, 2848–2851. [CrossRef]
59. Pace, G.; Stefankiewicz, A.; Harrowfield, J.; Lehn, J.-M.; Samor, P. Self-Assembly of Alkoxy-Substituted Bis(hydrazone)-Based Organic Ligands and of a Metallosupramolecular Grid on Graphite. *Chem. Phys. Chem.* **2009**, *10*, 699–705. [CrossRef] [PubMed]
60. Ruben, M.; Lehn, J.-M.; Müller, P. Addressing metal centres in supramolecular assemblies. *Chem. Soc. Rev.* **2006**, *35*, 1056–1067. [CrossRef] [PubMed]
61. Caronna, T.; Fronza, G.; Minisci, F.; Porta, O. Homolytic Acylation of Protonated Pyridine and Pyrazine Derivatives. *J. Chem. Soc. Perkin Trans. 2* **1972**, 2035–3038. [CrossRef]
62. Moroz, Y.S.; Demeshko, S.; Haukka, M.; Mokhir, A.; Mitra, U.; Stocker, M.; Müller, P.; Meyer, F.; Fritsky, I.O. Regular High-Nuclearity Species from Square Building Blocks: A Triangular 3 × [2 × 2] Ni_{12} Complex Generated by the Self-assembly of Three [2 × 2] Ni_4 Molecular Grids. *Inorg. Chem.* **2012**, *51*, 7445–7447. [CrossRef] [PubMed]

63. Sachse, A.; Demeshko, S.; Dechert, S.; Daebel, V.; Lange, A.; Meyer, F. Highly preorganized pyrazolate-bridged palladium(II) and nickel(II) complexes in bimetallic norbornene polymerization. *Dalton Trans.* **2010**, *39*, 3903–3914. [CrossRef] [PubMed]
64. Moroz, Y.S.; Kulon, K.; Haukka, M.; Gumienna-Kontecka, E.; Kozłowski, H.; Meyer, F.; Fritsky, I.O. Synthesis and Structure of [2 × 2] Molecular Grid Copper(II) and Nickel(II) Complexes with a New Polydentate Oxime-Containing Schiff Base Ligand. *Inorg. Chem.* **2008**, *47*, 5656–5665. [CrossRef] [PubMed]
65. Klingele, J.; Prikhod'ko, A.I.; Leibeling, G.; Demeshko, S.; Dechert, S.; Meyer, F. Pyrazolate-based copper(II) and nickel(II) [2 × 2] grid complexes: Protonation-dependent self-assembly, structures and properties. *Dalton Trans.* **2007**, 2003–2013. [CrossRef] [PubMed]
66. Cao, X.-Y.; Harrowfield, J.; Nitschke, J.; Ramírez, J.; Stadler, A.-M.; Kyritsakas-Gruber, N.; Madalan, A.; Rissanen, K.; Russo, L.; Vaughan, G.; et al. Generation of [2 × 2] Grid Metallosupramolecular Architectures from Preformed Ditopic Bis(acylhydrazone) Ligands and through Component Self-Assembly. *Eur. J. Inorg. Chem.* **2007**, *2007*, 2944–2965. [CrossRef]
67. Dinolfo, P.H.; Hupp, J.T. Tetra-Rhenium Molecular Rectangles as Organizational Motifs for the Investigation of Ligand-Centered Mixed Valency: Three Examples of Full Delocalization. *J. Am. Chem. Soc.* **2004**, *126*, 16814–16819. [CrossRef] [PubMed]
68. Dinolfo, P.H.; Williams, M.E.; Stern, C.L.; Hupp, J.T. Rhenium-Based Molecular Rectangles as Frameworks for Ligand-Centered Mixed Valency and Optical Electron Transfer. *J. Am. Chem. Soc.* **2004**, *126*, 12989–13001. [CrossRef] [PubMed]
69. Wu, J.-Y.; Thanasekaran, P.; Cheng, Y.-W.; Lee, C.-C.; Manimaran, B.; Rajendran, T.; Liao, R.-T.; Lee, G.-H.; Peng, S.-M.; Lu, K.-L. Unprecedented Reduction of 2,2′-Bipyrimidine in a One-Pot Synthesis of Neutral Rhenium(I)-Based Molecular Rectangles. *Organometallics* **2008**, *27*, 2141–2144. [CrossRef]
70. Dinolfo, P.H.; Lee, S.J.; Coropceanu, V.; Bredas, J.-L.; Hupp, J.T. Borderline Class II/III Ligand-Centered Mixed Valency in a Porphyrinic Molecular Rectangle. *Inorg. Chem.* **2005**, *44*, 5789–5797. [CrossRef] [PubMed]
71. Low, P.J.; Brown, N.J. Electronic Interactions Between and Through Covalently-Bonded Polymetallic Complexes. *J. Clust. Sci.* **2010**, *21*, 235–278. [CrossRef]
72. Mücke, P.; Winter, R.F.; Novak, I.; Kowalski, K. Synthesis, spectroelectrochemistry and electronic structure calculations of 4-(2-ferrocenylvinyl)-[2.2]-paracyclophane and 4,12-di-(2-ferrocenylvinyl)-[2.2]-paracyclophane. *J. Organomet. Chem.* **2012**, *717*, 14–22. [CrossRef]
73. Safin, D.A.; Babashkina, M.G.; Bolte, M.; Mitoraj, M.P.; Klein, A. Metal ion influences distortion of the ligand in the structure of $[M\{2\text{-}MeO(O)CC_6H_4NHC(S)NP(S)(OiPr)_2\}_2]$ ($M = Zn^{II}$, Cd^{II}) complexes: A driving force for the intermolecular aggregation. *Dalton Trans.* **2015**, *44*, 14101–14109. [CrossRef] [PubMed]
74. Burla, M.C.; Caliandro, R.; Camalli, M.; Carrozzini, B.; Cascarano, G.L.; Giacovazzo, C.; Mazzone, A.; Polidori, G.; Spagna, R. *Sir-2011, A Program for Automatic Solution and Refinement of Crystal Structures*; CNR Institute of Crystallography: Bari, Italy, 2012.
75. Altomare, A.; Cascarano, G.; Giacovazzo, C.; Guagliardi, A.; Burla, M.C.; Polidori, G.; Camalli, M. *Sir-92, A Program for Automatic Solution and Refinement of Crystal Structures*; CNR Institute of Crystallography: Bari, Italy, 1994.
76. Sheldrick, G.M. *SHELXL-2013. Program for the Refinement of Crystal Structures*; University of Göttingen: Göttingen, Germany, 2008.
77. Sheldrick, G.M. *SHELXL-97. Program for the Refinement of Crystal Structures*; University of Göttingen: Göttingen, Germany, 2008.
78. *X-Red 1.07*; Stoe &Cie GmbH: Darmstadt, Germany, 1996.
79. *X-Shape 1.0.1*; Stoe &Cie GmbH: Darmstadt, Germany, 1996.
80. Spek, A.L. *PLATON* SQUEEZE: A tool for the calculation of the disordered solvent contribution to the calculated structure factors. *Acta Cryst.* **2015**, *C71*, 9–18. [CrossRef]
81. Spek, A.L. *PLATON, A Multipurpose Crystallographic Tool*; Utrecht University: Utrecht, The Netherlands, 1998.
82. Waltersperger, S.; Olieric, V.; Pradervand, C.; Glettig, W.; Salathe, M.; Fuchs, M.R.; Curtin, A.; Wang, X.; Ebner, S.; Panepucci, E.; et al. PRIGo: A new multi-axis goniometer for macromolecular crystallography. *J. Synchrotron Radiat.* **2015**, *22*, 895–900. [CrossRef] [PubMed]
83. Kabsch, W. Integration, scaling, space-group assignment and post-refinement. *Acta Crystallogr. Sect. D Biol. Crystallogr.* **2010**, *66*, 133–144. [CrossRef] [PubMed]

84. Weigend, F. Accurate Coulomb-fitting basis sets for H to Rn. *Phys. Chem. Chem. Phys.* **2006**, *8*, 1057–1065. [CrossRef] [PubMed]
85. TURBOMOLE V7.0 2015, a Development of University of Karlsruhe and Forschungszentrum Karlsruhe GmbH, 1989–2007, TURBOMOLE GmbH. 2007. Available online: http://www.turbomole.com (accessed on 15 June 2015).
86. Steffen, C.; Thomas, K.; Huniar, U.; Hellweg, A.; Rubner, O.; Schroer, A. TmoleX—A Graphical User Interface for TURBOMOLE. *J. Comput. Chem.* **2010**, *31*, 2967–2970. [CrossRef] [PubMed]
87. Schäfer, A.; Horn, H.; Ahlrichs, R. Fully optimized contracted Gaussian basis sets for atoms Li to Kr. *J. Chem. Phys.* **1992**, *97*, 2571–2577. [CrossRef]
88. Schäfer, A.; Huber, C.; Ahlrichs, R. Fully optimized contracted Gaussian basis sets of triple zeta valence quality for atoms Li to Kr. *J. Chem. Phys.* **1994**, *100*, 5829–5835. [CrossRef]
89. Becke, A.D. Density-functional exchange-energy approximation with correct asymptotic behavior. *Phys. Rev. A* **1988**, *38*, 3098–3100. [CrossRef]